

DESY SR-80/06
June 1980

EXAFS: POSSIBILITIES, ADVANTAGES AND LIMITATIONS
FOR THE INVESTIGATION OF LOCAL ORDER IN METALLIC GLASSES

by

R. Haensel, P. Rabe, G. Tolkiehn and A. Werner
Institut für Experimentalphysik der Universität Kiel

Eigentum der Property of	DESY	Bibliothek library
Zugang: Accessions:	20. JUNI 1980	
Leihfrist: Loan period:	7	Tage days

DESY behält sich alle Rechte für den Fall der Schutzrechtserteilung und für die wirtschaftliche Verwertung der in diesem Bericht enthaltenen Informationen vor.

DESY reserves all rights for commercial use of information included in this report, especially in case of apply for or grant of patents.

To be sure that your preprints are promptly included in the
HIGH ENERGY PHYSICS INDEX ,
send them to the following address (if possible by air mail) :

DESY
Bibliothek
Notkestrasse 85
2 Hamburg 52
Germany

EXAFS: POSSIBILITIES, ADVANTAGES AND LIMITATIONS FOR THE INVESTIGATION OF LOCAL ORDER IN METALLIC GLASSES

R. Haensel, P. Rabe, G. Tolkiehn
and A. Werner

Institut für Experimentalphysik
der Universität Kiel, D 2300 Kiel 1,
F.R. Germany

ABSTRACT. Throughout this book many examples for the close relationship between the macroscopic properties and the local structure of liquid and amorphous metals and alloys are given. Complementing the conventional X-ray, electron and neutron scattering techniques the analysis of the "Extended X-ray Absorption Fine Structure" (EXAFS) has been developed to a reliable method for structural analysis. Although the phenomenon is known since the thirties of the century, its application for the determination of local geometrical parameters has only been introduced about ten years ago. The development of the method has been greatly stimulated by extensive theoretical work, e.g. more refined calculations of complex scattering amplitudes and by the availability of synchrotron radiation as an intense X-ray continuum source. Two aspects are discussed in this paper: i) The basic principles of EXAFS and the usual data evaluation techniques demonstrated for crystalline Fe; ii) Applications on amorphous systems, the modifications of the data evaluation due to nonsymmetric pair distributions and the comparison with other methods for structure determination.

Proc. NATO Advanced Study Institute "Liquid and Amorphous Metals", ed. E. Lüscher (D. Reidel, Dodrecht) to be published

1. INTRODUCTION

Since many decades X-rays are used in the investigation of the geometrical and the electronic structure of matter. Whereas diffraction studies are strongly related to the geometrical structure, absorption and its secondary effects are normally used to probe the electronic structure. EXAFS combines these two fields, investigating a scattering phenomenon to deduce geometrical structure informations by means of absorption measurements.

The roots of the method go back to the thirties when Kronig (1) tried to understand the origin of the fine structure observed in the energy range up to several hundred eV above the absorption edges. As an example Fig.1 (upper curve) shows the K-absorption spectrum of metallic Fe.

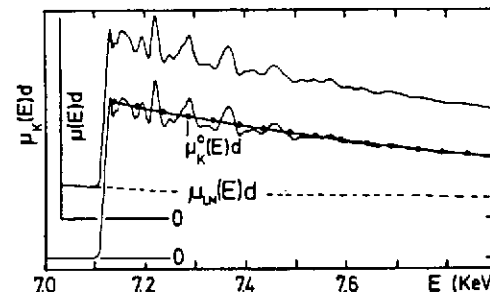


Fig.1 Fe (80K) absorption spectrum before (upper curve) and after (lower curve) subtraction of $\mu_{LM}(E)d$ (2)

EXAFS can be described as an electron diffraction process, where the electron source is the absorbing atom. The final state wave function of the excited state is formed from the outgoing photoelectron wave and the parts of it, which are backscattered from the surrounding atoms. Outgoing and backscattered waves interfere near the excited atom. According to Fermi's Golden Rule the photoabsorption coefficient $\mu(E)$ depends on the density of final states $\rho(E)$ and transition matrix element $M(E)$

$$\mu(E) \sim \rho(E) \cdot |M(E)|^2 \quad (1)$$

E is the photon energy. The term $\rho(E)$ has a monotonic behaviour except in the region near the edge. The ma-

trix element $M(E)$ represents the overlap of the initial and final state wave functions at the central atom. This overlap depends on the relative phase of outgoing and scattered wave and can be changed by tuning the wavelength (kinetic energy) of the photoelectron wave.

We express the absorption coefficient μ by

$$\mu = \mu_K^0(1 + \chi) + \mu_{LM} \quad (2)$$

where μ_K^0 is the monotonous absorption coefficient due to the excitation of the K -electrons of an isolated atom and μ_{LM} that of the weaker bound electrons (see Fig.1). χ represents the modulating part of the absorption coefficient, specific for the EXAFS modulation. About ten years ago Lytle, Sayers and Stern (3) demonstrated the usefulness of EXAFS to probe the local geometrical structure in matter. By their efforts they initiated great improvements of the theoretical background for a quantitative interpretation of the EXAFS data (4-10). A special impetus was given to the method by the availability of synchrotron radiation as an intense X-ray continuum source. The brightness of a synchrotron radiation source is superior to the bremsstrahlung intensity of a conventional X-ray generator by several orders of magnitude (11). A typical experimental setup is described in ref. (12).

2. BASIC CONSIDERATIONS

As has been mentioned above EXAFS originates from a modulation of the transition matrix element $M(E)$ caused by the scattering of the photoelectron wave. The kinetic energy of the photoelectrons E_{kin} is

$$E_{kin} = E - E_0 \quad (3)$$

where E is the photon energy and E_0 the binding energy. For the following it is convenient to introduce the wave number k which is calculated from

$$k = \sqrt{\frac{2m}{\hbar^2} E_{kin}} \quad (4)$$

The EXAFS above K -edges for unoriented samples can be written as (4-10)

$$\chi(k) = \sum_j A_j(k) \cdot \sin(2kR_j + \alpha_j(k)) \quad (5a)$$

with

$$A_j(k) = -\frac{1}{k} \frac{N_j}{R_j^2} \cdot |f_j(\pi, k)| \cdot e^{-R_j/\lambda} e^{-2\sigma_j^2 k^2} \quad (5b)$$

and

$$\alpha_j(k) = 2\delta_j(k) + \arg f_j(\pi, k) \quad (5c)$$

The summation is carried out over all coordination shells j . N_j is the number of identical atoms in the scattering shell j at the distance R_j ; $|f_j(\pi, k)|$ is the backscattering amplitude characteristic for the scattering atom; $\alpha_j(k)$ is the scattering phase, consisting of the phase shift $\arg f_j(\pi, k)$ due to the potential of the scatterer and the j phase shift $\delta_j(k)$ of the central atom. The first exponential in eq. (5b) describes the finite range of the photoelectron wave, the second exponential is a Debye-Waller factor and describes the disorder (dynamical (thermal) or static (structural)) with mean square relative displacements σ_j^2 . The $\chi(k)$ determined from the absorption spectrum of Fe is shown in Fig.2. The original data have been reduced as discussed in detail elsewhere (13).

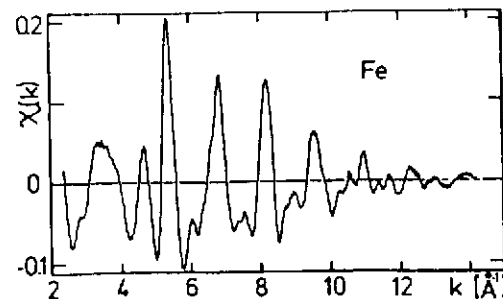


Fig.2:
 $\chi(k)$ extracted from the Fe absorption spectrum in Fig.1 (2)

In the following we will discuss in more detail the different ingredients of the EXAFS formula in eq.(5).

a) The argument of the sine term: It contains the information about distances R_j between the central atom and the surrounding scatterers. The frequency of $\chi(k)$ in k -space is modified by the k -dependent parts of the phase $\alpha_j(k)$. Its exact knowledge therefore is obviously important for the absolute determination of distances from EXAFS data. These phase shifts mainly depend on the atomic number of the central and the scattering atoms. The chemical bonding character only plays a minor role (chemical transferability) (13,14).

Two ways are possible to obtain the phase shifts $\alpha_j(k)$. They can simply be determined by calculated values of $\delta_1(k)$ and $\arg f(\pi, k)$. Examples obtained from Lee and Beni (7) are shown in Fig.3.

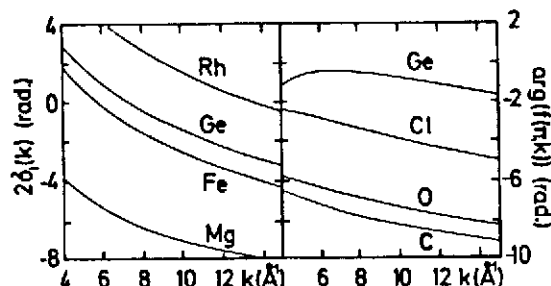


Fig.3: Scattering phases taken from Lee and Beni (7)

Alternatively the chemical transferability can be used to obtain the phase from EXAFS measurements of a crystallographically well known compound. Utilizing these phase shifts in systems of unknown geometry yields typical accuracies in the determination of bond lengths of $\pm 0.02 \text{ \AA}$. Changes of interatomic distances for atom pairs in comparable chemical environments due to phase transitions (e.g. amorphous-crystalline (15)) or to applied external forces (e.g. pressure (16)) may yield even higher accuracies. In special cases accuracies of $\pm 0.003 \text{ \AA}$ have been obtained (17).

b) The amplitude: The k -dependence of the backscattering amplitude $|f_j(\pi, k)|$ is specific for the scattering atom. Calculated values for $|f_j(\pi, k)|$ are shown in Fig.4 (10). For light elements like F $|f_j(\pi, k)|$ is a monotonically decreasing function for increasing k .

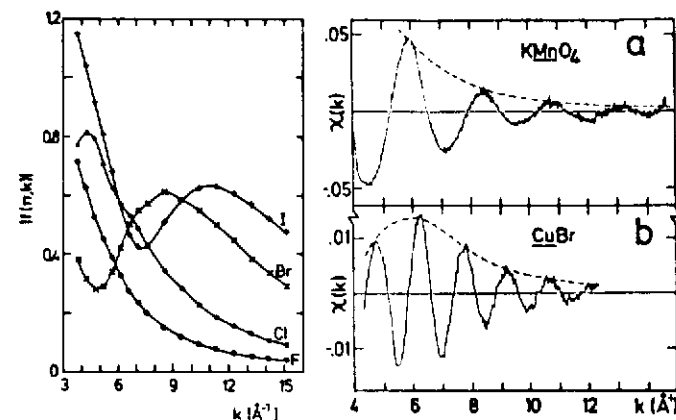


Fig.4 (left side): Scattering amplitudes obtained by Teo and Lee (10)
Fig.5 (right side): EXAFS at the K-edges of a) Mn in KMnO_4 (18) and b) Cu in CuBr (13)

For heavier atoms like Br $|f(\pi, k)|$ shows a maximum around $k \sim 8 \text{ \AA}^{-1}$. For even heavier elements the form of the backscattering amplitude becomes more complicated. A rough inspection of the EXAFS spectrum immediately can give some information about the type of the scattering atom. To illustrate this we compare in Fig.5 the EXAFS spectra of KMnO_4 and CuBr . The envelope functions show the expected k -dependent behaviour for light (O in KMnO_4 (a)) and heavy (Br in CuBr (b)) scatterers respectively.

The exponential $\exp(-2\sigma^2 k^2)$ describes the damping of the EXAFS spectrum towards high k values. This simple term is valid for the case of crystalline systems at low temperature, where the R_j -values of the discrete coordination shells are only smeared out by a small Gaussian broadening. Generally σ depends on the temperature. It increases with interatomic distances. Consequently the contributions from the second and higher coordination shells in the EXAFS spectrum decay much faster at higher k values (19,20). For large Gaussian broadenings or for asymmetric pair distribution functions, the simple exponential has to be modified by a more complicated term (21). This will be

discussed in section 4. The mean free path λ of the photoelectron wave in the second exponential of eq. (5b) depends on the lifetime of the core hole and the elastic and inelastic scattering of the photoelectrons in the environment of the central atom. Thus the range from which informations are carried in the EXAFS is confined to the immediate neighbourhood of the central atom, typically in the order of 6 Å.

The absolute determination of the coordination number N_j requires the precise knowledge of all other terms influencing the amplitudes of EXAFS. Even if all these values are known, a comparison of theoretical and experimental EXAFS spectra leads to inconsistencies. A reason for this is the assumption in the eq. (5), that all excited electrons coherently contribute to the interference effect. Other processes such as multielectron excitation are neglected in this model (22,23). Using the transferability of amplitude functions $A_j(k)$ (eq.6b) between experimental spectra in the sense as discussed for phases above typical accuracies of 10% can be achieved.

3. DATA EVALUATION

In simple cases with only one scattering shell the data reduction can be directly started from the EXAFS spectra in k -space. A fit with parametrized envelope functions $A_j(k)$ and phases $\alpha_j(k)$ can be applied to the experimental spectra. The increasing number of parameters in systems with more than one scattering shell limits the applicability of this technique. The most widely used method to separate the different contributions is a Fourier transform of $\chi(k)$ to real space (3). Each term in eq. (5) attributed to scatterers in a distance R_j shows up as a peak in the magnitude of the Fourier transform $F(r)$ (see Fig.6a). The magnitudes of these peaks are characterized by $A_j(k)$. The positions are determined by the argument of the sine function. According to the phase shift $\alpha_j(k)$ the positions of the peaks in $|F(r)|$ differ from the interatomic distances R_j by 0.2 to 0.5 Å.

There are several problems connected with the Fourier transform technique: The fact that only a limited k -range can be used (overlap of density of states below $k \sim 3\text{Å}^{-1}$ the damping of $\chi(k)$ at higher k -values due to the shape of $|E_j(r, k)|$ and the $\exp(-2\sigma^2 k^2)$ term) causes a broadening of the structure

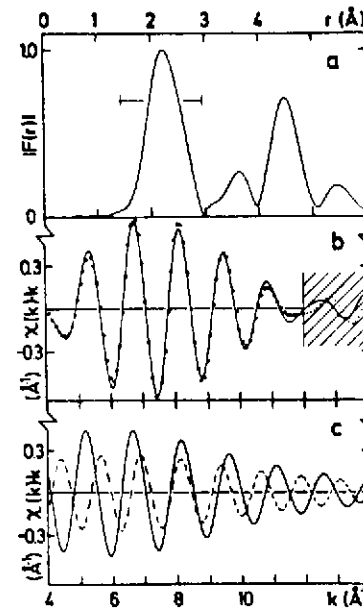


Fig.6:

- a) Magnitude of the Fourier transform of EXAFS of Fe at the K-edge (80K)
- b) Solid line: back transform of the first peak in a) and dotted line the best parameter fit
- c) From parameter fit obtained contribution for the first (solid line) and the second (dashed line) scattering shell

res in $|F(r)|$; cutoff effects lead to lobes which can interfere with the real structures. Nevertheless, the Fourier transform yields a separation of the contributions to $\chi(k)$ with different frequencies and can serve as a starting point for a more refined data analysis.

We demonstrate this with the EXAFS spectrum of Fe (Fig.2). The next neighbours (bcc lattice) of the central Fe atom are two close lying Fe-shells. The first pronounced peak in $|F(r)|$ at 2.1 Å (Fig.6a) is a superposition of contributions from both shells. Fig.6b (solid curve) shows the result of an inverse Fourier transform to k -space over the range indicated by a bar in $|F(r)|$. A parameter fit (Fig.6b dotted line) for two shells using calculated phase shifts and backscattering amplitudes has been included (dots). The single contributions of the first two shells extracted from this fit are displayed in Fig.8c.

Table I: Structural parameters of crystalline Fe

Shell	$R_E (\text{\AA})$	N_E	$R_C (\text{\AA})$	N_C
1	2.44	8.16	2.40	8
2	2.84	6.61	2.87	6

E values: EXAFS data

D values: X-ray diffraction data (24)

The discrepancies between the absolute distances determined by EXAFS (R_E) and by X-ray diffraction (R_D) are larger than the accuracies stated above. They are due to the limited accuracies of the theoretical phases. Note, however, that the differences between these shells are in excellent agreement between both methods. The influence of the phases is cancelled in this case.

A special advantage that EXAFS has to offer is the freedom to select the central atom by measuring EXAFS above the absorption edge of this element. This simplifies the structure analysis from EXAFS for multicomponent systems as compared to X-ray diffraction studies. In the latter case in a system with N different types of scattering atoms the structure factor is caused by a superposition of $N(N+1)/2$ partial pair distribution functions. For EXAFS the corresponding number reduces to N .

4. EXAFS RESULTS ON METALLIC GLASSES

Before we summarize applications of EXAFS to metallic glasses we briefly discuss the consequences of the degree of disorder on experimental spectra of amorphous Ge. Recent measurements of the EXAFS of a-Ge showed contributions from only the nearest neighbours (15,25). In contrast electron diffraction experiments (26) showed evidence for the first and second coordination shells. Although in apparent discrepancy both results are compatible with calculations based on the continuous random network model (27).

A careful analysis of the EXAFS data, especially of σ^2 of the first two shells of c-Ge and of the first shell of a-Ge showed, that the reason for the suppression of the second shell of a-Ge is the larger sensitivity of EXAFS to static and dynamic disorder compared to other techniques (15). This effect leads to a complete decay of the amplitude of these contributions beyond $k \sim 3 \text{\AA}^{-1}$. Since the range below $k \sim 3 \text{\AA}^{-1}$ cannot be used for the evaluation of the EXAFS data, the information about the second neighbour shell in a-Ge is permanently lost. This finding clearly demonstrates the high sensitivity of the EXAFS method to disorder.

Up to now we have described the pair distribution by a sum of δ -functions (static part $p_j(r)$) localized at R_j which are convoluted by Gaussians due to thermal broadening. For metallic glasses the static part of the distribution has to be replaced by a continuous distribution, asymmetric in the range of nearest neighbours. For an arbitrary pair distribution $p_j(r)$ the EXAFS has to be described by (21,28)

$$\chi(k) = \sum_j A_j(k) V_j(k) \sin \left\{ 2k \left(R_j - \frac{\arg V_j(k)}{2k} \right) + \alpha_j(k) \right\} \quad (6)$$

where $V_j(k)$ is the Fourier transform of

$$v_j(r) = \frac{p_j(r)}{r^2} \exp(-2r/\lambda) \quad (7)$$

The influence of magnitude and phase of $V_j(k)$ on the analysis of the local order can easily be demonstrated for an exponential distribution

$$v_j(r) = \exp\left(-\frac{r-R_j}{a}\right) \quad \text{for } r > R_j$$

and $\quad = 0 \quad \text{for } r \text{ elsewhere} \quad (8)$

This form of $v_j(r)$ serves in the following as an approximation of the pair distribution of metallic glasses (2,28). The most severe consequence for the determination of distances is the additional k -dependent term $(1/2k) \arg V_j(k)$. It decreases monotonically from a at $k=0$ to zero for $k \rightarrow \infty$. This means that a different weighting of EXAFS in different k -ranges pretends different interatomic distances, if eq.(5) is

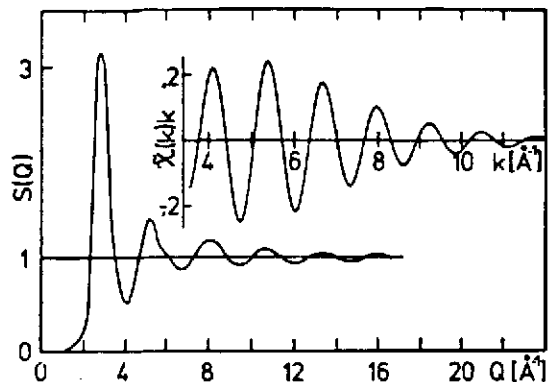


Fig. 7: $S(Q)$ structure factor for $\text{Fe}_{80}\text{B}_{20}$ obtained from X-ray diffraction; $\chi(k)$ EXAFS of $\text{Fe}_{80}\text{B}_{20}$ obtained from a two shell parameter fit to experimental data (Fig. 9a) and modified to $\alpha(k) = 0$

used. The same argument holds in a comparison of EXAFS with X-ray diffraction. This is demonstrated in Fig. 7. It shows the diffraction structure factor $S(Q)$ (29) together with the EXAFS (28) of $\text{Fe}_{80}\text{B}_{20}$. Whereas $S(Q)$ has its main contribution at low Q -values the range where EXAFS is observed and can be interpreted is confined to $k > 3 \text{ \AA}^{-1}$ (note that $Q = 2k$). Therefore, neglecting the asymmetry of $p_j(r)$ for metallic glasses yields for EXAFS distances which are typically 0.1 \AA smaller than those from X-ray scattering.

The experimental results for $\text{Fe}_{80}\text{B}_{20}$ are shown in Fig. 8 and in Table II. The Fourier transform (Fig. 8b) is dominated by a maximum at 2 \AA , which is a superposition of contributions from the nearest Fe- and B-neighbours. All higher coordination shells are substantially suppressed due to higher disorder through the effect described previously for Ge. Isolating the contributions contained in the first maximum by an inverse Fourier transformation of $|F(r)|$ for the range of $0.8 - 2.75 \text{ \AA}$ into k -space allows a separation of the partial Fe- and B-contributions with a two shell fit

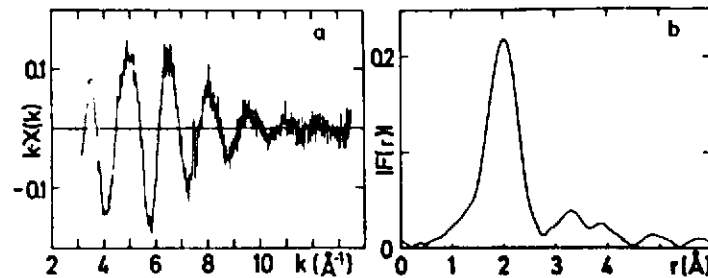


Fig. 8: a) EXAFS of $\text{Fe}_{80}\text{B}_{20}$ above the Fe K-edge; b) Magnitude of the Fourier transform of a.

Table II: Structural parameters for the nearest neighbours in $\text{Fe}_{80}\text{B}_{20}$

Shell	R_E	N_E	σ_E^2	R_E^C	N_E^C	R_D	N_D
B	1.96	1.2	0.009	2.06	2.2		
Fe	2.46	4.5	0.010	2.55	8.22	2.57	1.19

E values: after a parameter fit using eq. (5)

c values: after correcting for the asymmetric distribution (eq. 6)

D values: X-ray diffraction data by Waseda and Chen (29)

(see Fig. 9). The results using eq. (5) and experimental phase shifts and backscattering amplitudes of Fe are compiled in Table II (R_E , N_E and σ_E^2). A comparison with corresponding data from Waseda and Chen (29) obtained from X-ray scattering (R_D and N_D in Table II) shows deviations in R and even more dramatic in N . As has been mentioned above this disagreement is due to the fact that an inappropriate Gaussian pair distribution has been used to analyze the data. Assuming an asymmetry parameter of $a = 0.17 \text{ \AA}$ which is consistent with DRP (dense random packing of hard spheres (30))

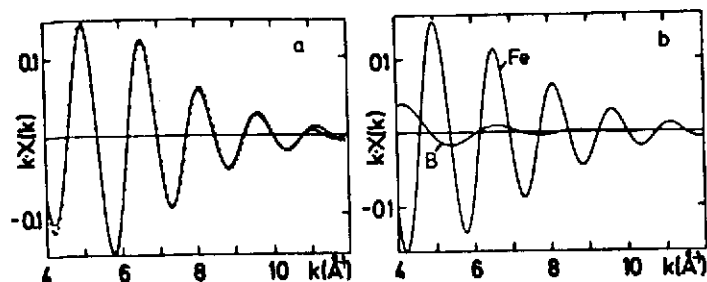


Fig.9: a) Solid line: back transform of the first peak in Fig.3b. Dotted line: Results of a parameter fit with contributions from the next Fe and B neighbours (part b)

distribution function for $\text{Fe}_{80}\text{B}_{20}$ the data of R_{Fe} and N_{Fe} can be corrected. The new values (R_{Fe}^c , N_{Fe}^c in Table II) are much closer to those of Waseda and Chen (29).

The first EXAFS measurements on metallic glasses have been performed by Hayes et al. (31) on $\text{Pd}_{80}\text{Ge}_{20}$ above the K-edge of the metalloid Ge. Their best fit of the data yields 8.6 nearest neighbours (Pd) around Ge with a distance of $2.49 \pm 0.01 \text{ \AA}$, slightly smaller than the value for crystalline PdGe (24). No evidence for Ge in the first coordination shell has been found in accordance with the Polk model (32) based on a DRPHS (dense random packing of single sized hard spheres) model. The small spread of $\pm 0.1 \text{ \AA}$ in the experimental data for the next neighbours distance, however, has been stated to be in contrast to this and to more refined model calculations (33). The latter model yielded a spread of 0.21 \AA . Thus Boudreaux (33) concluded that Hayes et al. (31) used an inappropriate pair correlation. Calculations (28) show that experimental data in fact can be approximated with eq.(5). As discussed above this yields N- and R-values smaller than those derived from X-ray diffraction. Furthermore one gets σ -values, which are smaller than the true widths of the asymmetric pair distribution. To conclude, differences in interatomic distances derived from EXAFS and X-ray scattering are an essential hint for the existence of a non-Gaussian pair distribution.

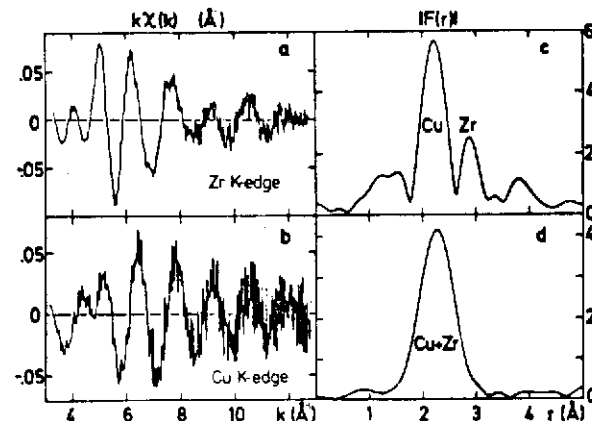


Fig.10: a) and b) EXAFS above the K-edges of Zr and Cu in the metallic glass $\text{Zr}_{54}\text{Cu}_{46}$; c) and d) the Fourier transform of a) and b) respectively

In contrast to the previous examples the K-edges EXAFS of both constituents have been investigated in $\text{Zr}_{54}\text{Cu}_{46}$ (2). The EXAFS above the K-edges of Zr and Cu are shown in Fig.10 a) and b) respectively. The parts c) and d) of Fig.10 show $|F(r)|$. Between 1.8 \AA and 3.2 \AA , two well separated maxima show up at 2.2 \AA and 2.8 \AA , which can be ascribed to the next Cu- and Zr-neighbours. The broader maximum at 2.3 \AA in d) is attributed to the Cu- and Zr-neighbours of the central Cu-atom. The single Cu- and Zr-contributions in the Zr K-edge EXAFS have been isolated by inverse Fourier transform of each peak in $|F(r)|$ separately. Fits with the general form of $\chi(k)$ (eq.(6)) with $a = 0.12 \text{ \AA}$ for Cu, but $a = 0$ for Zr and experimental phases and amplitudes using N, R and σ as free parameters yielded values which are in good agreement with X-ray diffraction data (see Table III). An inverse Fourier transform of the first peak in Fig.10 d) yields the Cu- and Zr-contributions simultaneously. This EXAFS has been fitted by eq.(5) using the R values of Zr-Cu determined above. The significantly larger Cu-Cu distance found in X-ray diffraction again points to an asymmetric distribution. To summarize we find coordination numbers in agreement with the stoichiometric composition of the alloy, but we

Table III: Structural parameters of $Zr_{54}Cu_{56}$

Central atom	Scatterer	R_E	N_E	R_D	N_D
Zr	Cu	2.74 ± 0.02^C	4.6 ± 1^C	2.75	5.0
	Zr	3.14 ± 0.02	5.1 ± 1	3.15	5.0
Cu	Cu	2.47 ± 0.03		2.53	5.8
	Zr	2.74 ± 0.03^C		2.75	5.6

E, c: see Table IV; D: X-diffraction data (34)

have different pair distribution characters, i.e. symmetric for Zr-Zr and asymmetric for Cu-Cu and Cu-Zr.

As a multicomponent system $Fe_{40}Ni_{40}B_{20}$ has been studied (2). Similar measurements have been performed by Wong et al. (35) on $Fe_{40}Ni_{40}B_{20-x}x$ (with x varying from 0 to 20 at %). Fig. 11 shows the data for $Fe_{40}Ni_{40}B_{20}$ (2) for both the EXAFS regions above the Fe and Ni K-edge. Similarly as for the $Fe_{80}B_{20}$ the $|F(r)|$ mainly contains one pronounced peak with a maximum at 2.08 Å, representing the nearest neighbour shell for the Fe- or Ni-atoms. We first consider the Fe K-edge spectrum. A comparison with the $Fe_{80}B_{20}$ data showed a good coincidence of the frequencies of the fine structure and hence the positions of the maxima in $|F(r)|$. The deviation is less than 0.02 Å. This leads to the statement, that replacement of 50% of the Fe-atoms by Ni-atoms does not alter the Fe vicinity significantly.

The amplitudes and phases of Fe and Ni are nearly identical and the Fe-Ni distances are comparable. This has the consequence that we cannot discriminate between Fe and Ni scatterers within our limits of accuracy. In the same way as previously done for $Fe_{80}B_{20}$ we perform an inverse transform of the first maximum back to k-space and by a parameter fit with eq. (5) using calculated backscattering amplitudes and phases we determine the R_E and N_E values for (Fe, Ni) and B neighbours (Table IV).

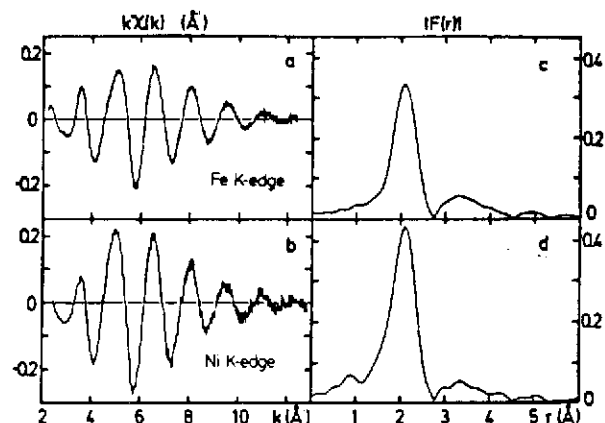


Fig. 11: a) and b) EXAFS contributions of $Fe_{40}Ni_{40}B_{20}$ above the K-edges of Fe and Ni; c) and d) the structural functions $|F(r)|$ belonging to a) and b)

The Fe-(Fe, Ni) distances R_E and the coordination numbers N_E are in good agreement with the corresponding Fe-Fe values for $Fe_{80}B_{20}$. This means that the pair correlation functions are the same in both cases. With an asymmetry parameter of $a = 0.17$ Å found for $Fe_{80}B_{20}$ an $R_E = 2.57$ Å is obtained. Analyzing the Ni EXAFS with eq. (5) the Ni-(Fe, Ni) distance R_E turns out to be the same as the Fe-(Fe, Ni) value. However, a significantly different coordination number N_E is observed, resulting in N_E (Ni-EXAFS)/ N_E (Fe-EXAFS) = 1.4.

There are two possible explanations for the behaviour: i) The number of (Fe, Ni) in the next neighbour shell of Ni is really higher by a factor of 1.4 as compared to the Fe-vicinity. ii) The coordination numbers are the same, but the asymmetry parameters for the distribution functions are different. The assumed asymmetry factor $a = 0.17$ Å for the Fe vicinity already enlarges $N_E = 4.9$ (from eq. (5)) to $N_E = 12$ (using eq. (6)). The same a -value applied to the Ni vicinity would yield a $N_E \sim 17$ atoms, certainly an un-

Table IV: Structural parameter of $\text{Fe}_{40}\text{Ni}_{40}\text{B}_{20}$

Central Atom	Scatterer	R_E (Å)	N_E	R_E^C	N_E^C
Fe	B	1.97			
	(Fe,Ni)	2.48	4.9	2.57	12
Ni	B	1.95			
	(Fe,Ni)	2.45	6.9	2.51	12

E values: after a parameter fit using eq.(5)

c values: after correcting for the asymmetric distribution (eq.6)

realistic number. Therefore, the solution ii) seems to be more appropriate. Assuming $N_E^C = 12$ for the Ni vicinity as well leads to an asymmetry factor $a = 0.11$ Å.

Independent of a more detailed analysis the data show distinct differences in the short range order around the Fe- and Ni-atoms in $\text{Fe}_{40}\text{Ni}_{40}\text{B}_{20}$. This necessitates the inclusion of chemical bonding effects in the description of the local structure.

Similar conclusions can also be drawn from the measurements on $\text{Fe}_{40}\text{Ni}_{40}\text{B}_{20-x}\text{P}_x$ by Wong et al. (35), who derived the fractional change ($\Delta\sigma^2/\sigma^2$) in disorder around the Fe and Ni atoms as a function of x and of the annealing temperature from the peak heights in $|F(r)|$. For $x = 0$, i.e. $\text{Fe}_{40}\text{Ni}_{40}\text{B}_{20}$ the disorder around the Fe atom is larger than that around the Ni atoms; Wong et al. (35) stated that the boron preferentially coordinates with Ni. On the other hand for $\text{Fe}_{40}\text{Ni}_{40}\text{P}_{20}$ phosphorous coordinates preferentially with Fe.

ACKNOWLEDGEMENTS

This work was supported by the Bundesministerium für Forschung und Technologie and the Deutsches Elektronen-Synchrotron DESY. The support by the members of the synchrotron radiation group at DESY is gratefully acknowledged. We thank Prof. Güntherodt (Basel) for providing samples used in our work. Finally thanks are

due to M. Höfelmeyer for a careful typing of the manuscript.

REFERENCES

1. R. de L. Kronig, Z.Phys. 70, 317 (1931); 75, 191 and 468 (1932)
2. A. Werner, Dr.rer.nat. thesis, Universität Kiel 1979
3. F.W. Lytle, in Adv. X-ray Analysis 9, 398 (1966) (Plenum Press)
D.E. Sayers, E.A. Stern and F.W. Lytle, Phys.Rev. Letters 27, 1204 (1971)
F.W. Lytle, D.E. Sayers and E.A. Stern, Phys.Rev. B 11, 4825 (1975)
E.A. Stern, D.E. Sayers and F.W. Lytle, Phys.Rev. B 11, 4836 (1975)
4. E.A. Stern, Phys.Rev.B 10, 3027 (1974)
5. C.A. Ashley and S. Doniach, Phys.Rev.B 11, 1279 (1975)
6. P.A. Lee and J.P. Pendry, Phys.Rev. 11, 2795 (1975)
7. P.A. Lee and G. Beni, Phys.Rev.B 15, 2862 (1977)
8. B.K. Teo, P.A. Lee, A.L. Simons and P. Eisenberger, J.Am.Chem.Soc. 99, 3854 (1977)
9. P.A. Lee, B.K. Teo and A.L. Simons, J.Am.Chem.Soc. 99, 3856 (1977)
10. B.K. Teo and P.A. Lee, J.Am.Chem.Soc. 101, 2815 (1979)
11. C. Kunz, ed., Synchrotron Radiation, Topics in Current Physics, Vol.10 (Springer Verlag Berlin, Heidelberg, New York, 1979)
12. P. Rabe, G. Tolkiehn and A. Werner, Nucl.Instr. Meth. (to be published, preprint DESY SR-79/23)
13. G. Martens, P. Rabe, N. Schwentner and A. Werner, Phys.Rev.B 17, 1481 (1978)

14. P.H. Citrin, P. Eisenberger and B.M. Kincaid, *Phys.Rev.Letters* 36, 1346 (1976)
15. P. Rabe, G. Tolkiehn and A. Werner, *J.Phys.C* 12 L545 (1979)
16. R. Ingalls, G.A. Garcia and E.A. Stern, *Phys.Rev. Letters* 40, 334 (1978)
17. G. Martens, P. Rabe, N. Schwentner and A. Werner, *Phys.Rev.Letters* 39, 1411 (1977)
18. P. Rabe, G. Tolkiehn and A. Werner, *J.Phys.C* 12, 1173 (1979)
19. G. Beni and P.M. Platzman, *Phys.Rev.B* 14, 1514 (1976)
20. W. Böhmer and P. Rabe, *J.Phys.C* 12, 2465 (1979)
21. P. Eisenberger and G.S. Brown, *Sol.State Comm.* 29, 481 (1979)
22. J.J. Rehr, E.A. Stern, R.L. Martin and E.R. Davidson, *Phys.Rev.B* 17, 560 (1978)
23. E.A. Stern, S.M. Heald and B. Bunker, *Phys.Rev. Letters* 42, 1372 (1979)
24. R.W. Wyckhoff, *Crystal Structures*, Vol.I (Interscience Publishers, 1963)
25. Unpublished results of S. Hunter, see T.M. Hayes, *J.Non-Cryst.Sol.* 31, 57 (1979)
26. J.F. Grazcyk and P. Chaudhari, *phys.stat.sol.(b)* 58, 163 (1973)
27. P. Chaudhari and D. Trunbull, *Science* 199, 11 (1978)
See also: Electronic Processes in Non-Crystalline Materials, 2nd edition by N.F. Mott and E.A. Davis (Clarendon Press, Oxford 1979) chapter 7
28. R. Haensel, P. Rabe, G. Tolkiehn and A. Werner (to be published)

29. Y. Waseda and H.S. Chen, *phys.stat.sol.(a)* 49, 387 (1978)
30. G.S. Cargill III, *Solid State Physics* Vol.30, 227 (1975) (Academic Press)
31. T.M. Hayes, J.W. Allen, J. Tauc, B.C. Giessen and J.J. Hauser, *Phys.Rev.Letters* 40, 1282 (1978)
32. D. Polk, *Acta Metall.* 20, 485 (1972)
33. D.S. Boudreaux, *Phys.Rev.* 18, 4039 (1978)
34. H.S. Chen and Y. Waseda, *phys.stat.sol.(a)* 51, 593 (1979)
35. J. Wong, F.W. Lytle, R.B. Gregor, H.H. Liebermann J.L. Walter and F.E. Luborsky, in Rapidly Quenched Metals III, ed. B. Cantor (The Metals Society, London 1978) Vol.II, p.345